FULL TITLE
ASP Conference Series, Vol. **VOLUME**, **YEAR OF PUBLICATION**
NAMES OF EDITORS

Exoplanet-Induced Chromospheric Activity: Realistic Light Curves from Solar-type Magnetic Fields

Steven R. Cranmer and Steven H. Saar

Harvard-Smithsonian Center for Astrophysics, 60 Garden Street, Cambridge, MA 02138, USA

Abstract. There is growing observational evidence for some kind of interaction between stars and close-in extrasolar giant planets. Shkolnik et al. reported variability in the chromospheric Ca H and K lines of HD 179949 and υ And that seemed to be phased with the planet's orbital period, instead of the stellar rotational period. However, the observations also indicate that the chromospheric light curves do not repeat exactly, which may be expected for a planet plowing through a variable stellar magnetic field. Using the complex solar magnetic field (modeled with the Potential Field Source Surface technique) as a guide, we simulate the shapes of light curves that would arise from planet-star interactions that are channeled along magnetic field lines. We also study the orbit-to-orbit variability of these light curves and how they vary from solar minimum (i.e., a more or less axisymmetric stretched dipole) to solar maximum (a superposition of many higher multipole moments) fields. Considering more complex magnetic fields introduces new difficulties in the interpretation of observations, but it may also lead to valuable new diagnostics of exoplanet magnetospheres.

1. Introduction

Many of the ∼200 known extrasolar planets are "Hot Jupiters" (i.e., giant planets with star-planet distances less than about 0.1 AU) that have been identified from perturbations in their host star's radial velocities. Other ways in which a close-in extrasolar giant planet (CEGP) can influence its star include tidal distortions and magnetic interactions. These effects can produce enhanced stellar flare activity (Rubenstein & Schaefer 2000), chromospheric and coronal emission (Cuntz et al. 2000), and magnetospheric radio emission (Zarka et al. 2001). Tidal and magnetic interactions have been proposed to explain similar phenomena observed in RS CVn close binary systems (e.g., Simon et al. 1980; Ferreira & Mendoza-Briceño 2005), stars with possibly unseen companions exhibiting "superflares" (Schaefer et al. 2000), and even in the aurora of Jupiter where there are magnetic connections to the inner Galilean moons (Clarke et al. 2002). We refer to Saar et al. (2004) for a recent review of observations (or the lack thereof) of various kinds of CEGP-star interactions and possible theoretical explanations for these effects.

In this presentation we focus on the chromospheric (Ca H & K line) enhancements on a star due to magnetic interactions between the stellar field and the CEGP's magnetosphere. We used the empirically derived solar magnetic field, as a function of the 11-year solar cycle, as a proxy for the field geometry and field strength of CEGP host stars. We simulated light curves that represent

the sum of the rotational modulation of the star's own H&K line emission and the added emission from the small set of flux tubes connected to the planet's magnetosphere.

2. Observed Ca H & K Enhancements

Several early attempts to identify planet-induced chromospheric emission (reviewed by Saar et al. 2004) were unsuccessful mainly because the observations were not designed specifically for this purpose. Shkolnik et al. (2003, 2005) used high-resolution ($\lambda/\Delta\lambda \sim 10^5$) Ca II H & K spectroscopy to identify two cases of chromospheric enhancement that are phased with the planet's orbit. HD 179949 (F8 V, $P_{\rm rot} \approx 9$ days) has a CEGP with $P_{\rm orb} = 3.092$ days, $M \sin i = 0.98\,M_{\rm Jup}$, and semimajor axis $d = 0.045$ AU. The Ca K enhancement for HD 179949 occurs at a phase shift $\Delta\phi$ of almost 0.2 *ahead* of the sub-planet point reaching stellar disk-center. This raised suspicions that the star's magnetic field may be swept back into a "Parker spiral" at the orbit of the CEGP, but for a solar-type magnetic field and wind this is unlikely. On the other hand, HD 179949 is more active than the Sun (e.g., $F_{\rm X}/F_\odot \sim 20$) and of earlier spectral type ($T_{\rm eff} \approx 6170$ K; Valenti & Fischer 2005) suggesting both the stellar magnetic structure and wind could be quite different from the solar case. Shkolnik et al.'s data from 2003 do not show the strong orbital modulation of the 2001–2002 data, but there is still a weak maximum at $\phi \sim 0.8$ in agreement with the earlier epochs. Similar data for υ And (F7 V, $P_{\rm rot} \approx 14$ days, $P_{\rm orb} = 4.6$ days) reveals a slightly weaker H & K amplitude, but a maximum with phase shift $\Delta\phi \approx 0.5$, i.e., when the planet is behind the star (see also Harrington et al. 2006).

3. Theoretical Explanations?

The periodicity and strength of the HD 179949 and υ And variations indicate that *magnetic interaction* is the most likely mechanism. Saar et al. (2004) found that other mechanisms such as tidal distortions or Io-like inductance would have produced even stronger modulations in other star-planet systems for which no planet-phased variations have been found (e.g., τ Boo). In addition, tidal distortions would have caused two peaks in the light curve per orbit, rather than just one as is observed. The energy released in the Ca H&K enhancement ($\sim 10^{27}$ erg/s) is similar to that released in typical solar flares. Ip et al. (2004) modeled CEGP magnetospheres and found that this level of power generation can be expected from magnetic reconnection in the most likely geometries.

McIvor et al. (2006) predicted the shapes of Ca H&K light curves consistent with magnetic field lines connecting a planet and an inclined, stretched dipolar stellar field. Phase shifts similar to that of HD 179949 can be reproduced by misalignment between magnetic and rotation axes. Also, Preusse et al. (2006) were able to model similar phase shifts by assuming the CEGP to be inside the star's Alfvén radius (i.e., where the Alfvén speed exceeds the outflow speed; $r \lesssim 10\,R_\odot$ for the solar wind) and that the perturbations travel from the planet to the star along the *longitudinally varying* inward Alfvén characteristics.

Magnetic interaction models depend on the product of the relative velocity between the two fields (known from the orbital dynamics), the stellar magnetic

field strength (which can be deduced from Zeeman splitting or estimated from known activity scalings), and the planetary magnetic field strength, which is not yet observed, though modeling progresses (e.g., Sánchez-Lavega 2004; Stevens 2005).

4. Exploratory Models

Our goal has been to produce more realistic simulations of Ca K light curves for a rotating solar-type star undergoing a CEGP magnetic interaction. We use modeled three-dimensional solar magnetic field configurations (as a function of the 11-year solar cycle) to simulate both the stellar and planetary light curve components. Observed maps of the photospheric magnetic flux were extrapolated into the extended corona using the Potential Field Source Surface (PFSS) method. The corona is assumed to remain current-free out to a spherical "source surface" at $R_{\rm ss} = 2.5\,R_\odot$ where the nonradial field components are set to zero, simulating the magnetohydrodynamic (MHD) expansion of the solar wind (e.g., Schatten et al. 1969; Altschuler & Newkirk 1969; Hoeksema & Scherrer 1986; Wang & Sheeley 1990).

The highest multipole components fall off the most rapidly with increasing height, resulting in the photospheric field being much more complex than the field at $r = R_{\rm ss}$. Data and reconstruction coefficients were obtained for 11 solar rotations (one per year over a solar cycle) from Wilcox Solar Observatory.[1] Somewhat arbitrarily, we used the solar magnetic field from the month of August in each of the years of solar cycle 22 (1986–1996); i.e., the specific Carrington Rotations 1778, 1792, 1805, 1819, 1832, 1845, 1859, 1872, 1886, 1899, and 1913.

The following subsections describe how the stellar (§ 4.1) and planetary (§ 4.2) light curve components were computed.

4.1. Stellar Light Curve

Figure 1 shows the variation of sunspot number[2] and Ca K-line emission over solar cycle 22. The larger number of sunspots at solar maximum corresponds directly to the larger number of chromospheric plage and active regions which enhance the disk-integrated K-line emission. The Ca K-line data came from daily observations at the Sacramento Peak Observatory of the U.S. Air Force Phillips Laboratory.[3] The Sac Peak K_3 index was divided by a fiducial wing-to-continuum ratio of 0.40 in order to obtain the same kind of core-to-wing intensity ratio used by Shkolnik et al. (2003, 2005). These values were then calibrated against the hemisphere-averaged magnetic flux densities $\langle B \rangle$ (measured at the solar surface) over the modeled epochs. We performed a similar fit between these two quantities as did Schrijver et al. (1989), and found

$$(I_{\rm core}/I_{\rm wing}) \;=\; 0.13 \;+ 0.024\langle B \rangle^{0.63} \qquad (1)$$

[1] http://sun.stanford.edu/∼wso/

[2] http://sidc.oma.be/sunspot-data/

[3] http://www.ngdc.noaa.gov/stp/SOLAR/ftpcalcium.html

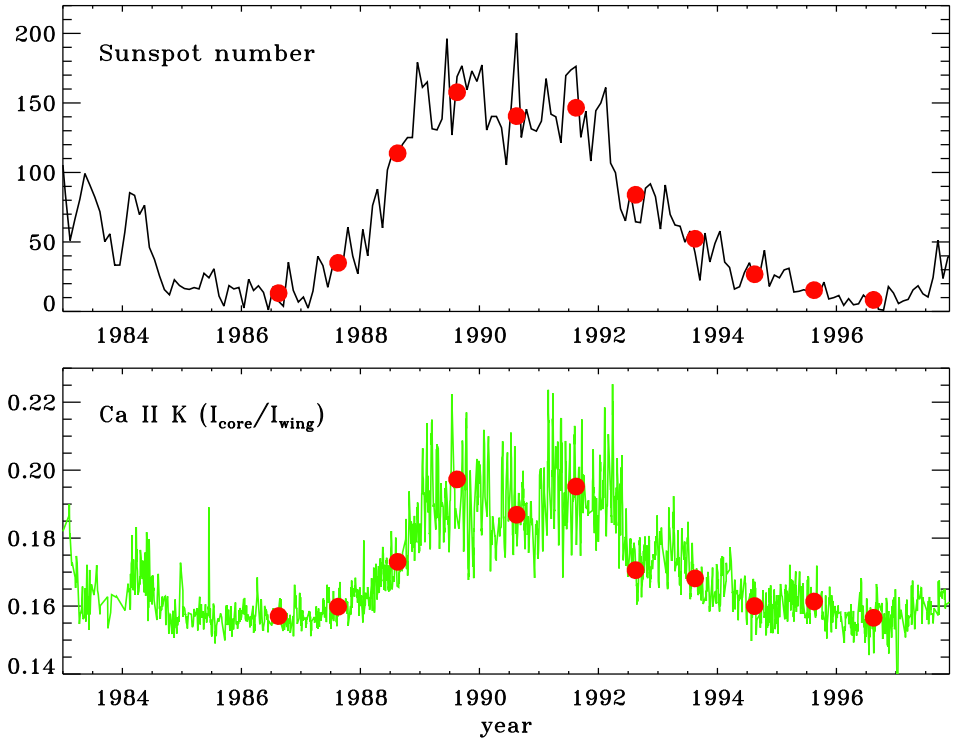

Figure 1. *Top:* monthly raw sunspot number over cycle 22. *Bottom:* Ca II K-line ratio of core to wing intensity (see text). Red points in both panels define the 11 specific solar rotations that we chose to model in detail.

where $\langle B \rangle$, measured in Gauss, was computed from the PFSS models over the 11 modeled rotations at times corresponding to the K-line observations. This relation was then used to compute the theoretical stellar-rotation light curves in Figures 3 and 4 from the "exactly known" photospheric magnetic fields.

4.2. Planetary Light Curve

To model the enhancement due to planet-star coupling, we assumed the power released in magnetic interaction scales as

$$P \sim \frac{B_* B_{\rm P}}{8\pi} \left(\pi r_{\rm mag}^2\right) V_{\rm rel} \tag{2}$$

where the stellar magnetic field (B_*) and planetary field ($B_{\rm P}$) are measured at the planet's magnetosphere, which has a projected area $\pi r_{\rm mag}^2$ intercepted by the stellar field (e.g., Saar et al. 2004). Later, we use $r_{\rm mag} \approx 5\,R_{\rm Jup}$, which was also assumed by Ip et al. (2004). The two magnetic fields move through one another at relative velocity $V_{\rm rel}$ ($\sim$100 km/s for HD 179949). We assumed that $B_{\rm P}$, $r_{\rm mag}$, and $V_{\rm rel}$ remain fixed over multiple rotations and the activity cycle, and thus that *time variations* in P are sensitive only to B_*.

For each of the 11 epochs, we created a fine grid of planetary longitudes (300 points around the circular orbit) defined relative to the fixed Carrington

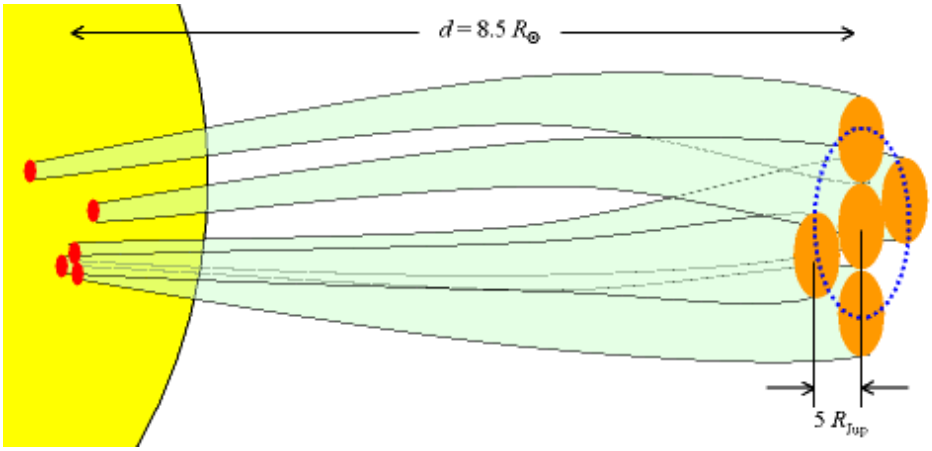

Figure 2. Cartoon illustrating the coarse array of magnetic flux tubes traced down from the CEGP magnetosphere to the stellar surface. Not to scale.

longitude coordinates of the modeled magnetic field. For each planetary position, we traced an envelope of 5 flux tubes from the planet's orbit ($d > R_{ss}$) down to the stellar surface. Figure 2 shows the cross-like configuration of flux tubes that we used to resolve the magnetosphere; note that the pattern of flux tube "footpoints" on the stellar surface is likely to have a more complicated shape. We used more than one flux tube so that "bifurcation" events (when the finite-sized magnetosphere connects down to two widely separated areas on the stellar surface) could be at least approximately resolved. Future work should of course use a more finely sampled envelope of flux tubes so that the detailed shapes of the resulting star spots can be computed.

The mapped flux tubes were then input into a time-resolved model of both the planet's orbit and the star's rotation. The instantaneous angular positions of the star, planet, and observer were tracked, and the angle θ (measured between the stellar surface normal at the flux-tube footpoint and the observer's line of sight) was computed as a function of time. The relative contribution from each flux tube was thus assumed to be proportional to the stellar field strength at the magnetosphere (B_*) modulated by the spot's projection factor; i.e.,

$$(I_{\rm core}/I_{\rm wing}) \propto \sum (B_* \cos\theta) \quad \text{(summed over 5 footpoints)} \tag{3}$$

The above procedure contains the assumption that the magnetic "communication" between star and planet is essentially instantaneous. This would be a valid assumption if the energy were carried by, e.g., suprathermal particles as in strong solar flares, but not if the energy had to propagate along more slowly as an MHD wave (see Preusse et al. 2006).

We adopted dynamical parameters roughly analogous to HD 179949 (e.g., $P_{\rm rot} = 2.9 P_{\rm orb}$, not an exact multiple), and we set the overall normalization for $I_{\rm core}/I_{\rm wing}$ to resemble the observed amplitude (Shkolnik et al. 2005). This arbitrary normalization is of course a weak point of the present models, but without a specific predictive model of the magnetic interaction not much more was possible.

5. Results

Figures 3 and 4 show the magnetic field configurations and light curves for the 11 modeled epochs. The overall polarity "flip" is evident over the 11-year solar cycle. Both the complete light curve (star plus planet) and just the stellar rotational component are shown in order to clearly see the planetary enhancement. The light curve is shown in detail over five planetary orbits. The planetary enhancements generally occur when the planet is in front of the star ($\phi \sim 0$) but occasional planetary enhancements occur at other phases, or are absent at phase zero. Rapid changes sometimes occur over less than 0.05 in phase (i.e., over just several hours in time). We also show a much coarser kind of "light curve" that was randomly sampled with 200 points spread over a time-span of 200 planetary orbits. In these plots, the stellar rotation light curve is not resolved except as a fuzzy "band" which the planetary enhancement tends to exceed around phase zero.

Because the amplitudes of *both* the stellar-rotation light curve and the planetary enhancements are larger at solar maximum than at solar minimum, there is no systematic trend for the planetary enhancement to "poke its head above the fuzz" more at either maximum or minimum. Thus, there does not seem to be any preferred cycle-phase for the planetary enhancement to be more or less distinguishable from the stellar rotational modulation.

Figure 5 shows some statistical properties of the light curves, with one point in each panel characterizing the variations over each of the 11 epochs. The minimum, maximum, and average intensity ratios ($I_{\rm core}/I_{\rm wing}$) were determined for the separate stellar and planetary light curves and correlated with one another. The tendency for the amplitudes of the stellar and planetary light curves to rise and fall together was discussed above and is evident in the direct correlations. Note specifically the nearly linear relationship between the maximum planet enhancement and the total (max − min) amplitude of the stellar light curve.

6. Conclusions

Some of the more interesting features of the modeled light curves are summarized here:

1. Because of the complex nature of the multipole fields, the modeled light curves do not repeat exactly from orbit to orbit, and sometimes the planetary enhancement seems to disappear altogether. This may be a possible explanation for the 2003 disappearance of the strong orbital modulation seen in 2001–2002 for HD 179949 (Shkolnik et al. 2005).

2. The planetary enhancements are often non-monotonic in shape (i.e., multiply peaked). This occurs because the "spots" on the stellar surface that connect to the planet's magnetosphere may be bifurcated or substantially swept around in longitude and/or latitude.

3. For sparsely sampled data, the inferred phase shift between light-curve maximum and planetary meridian-passage may range between -0.2 and $+0.2$.

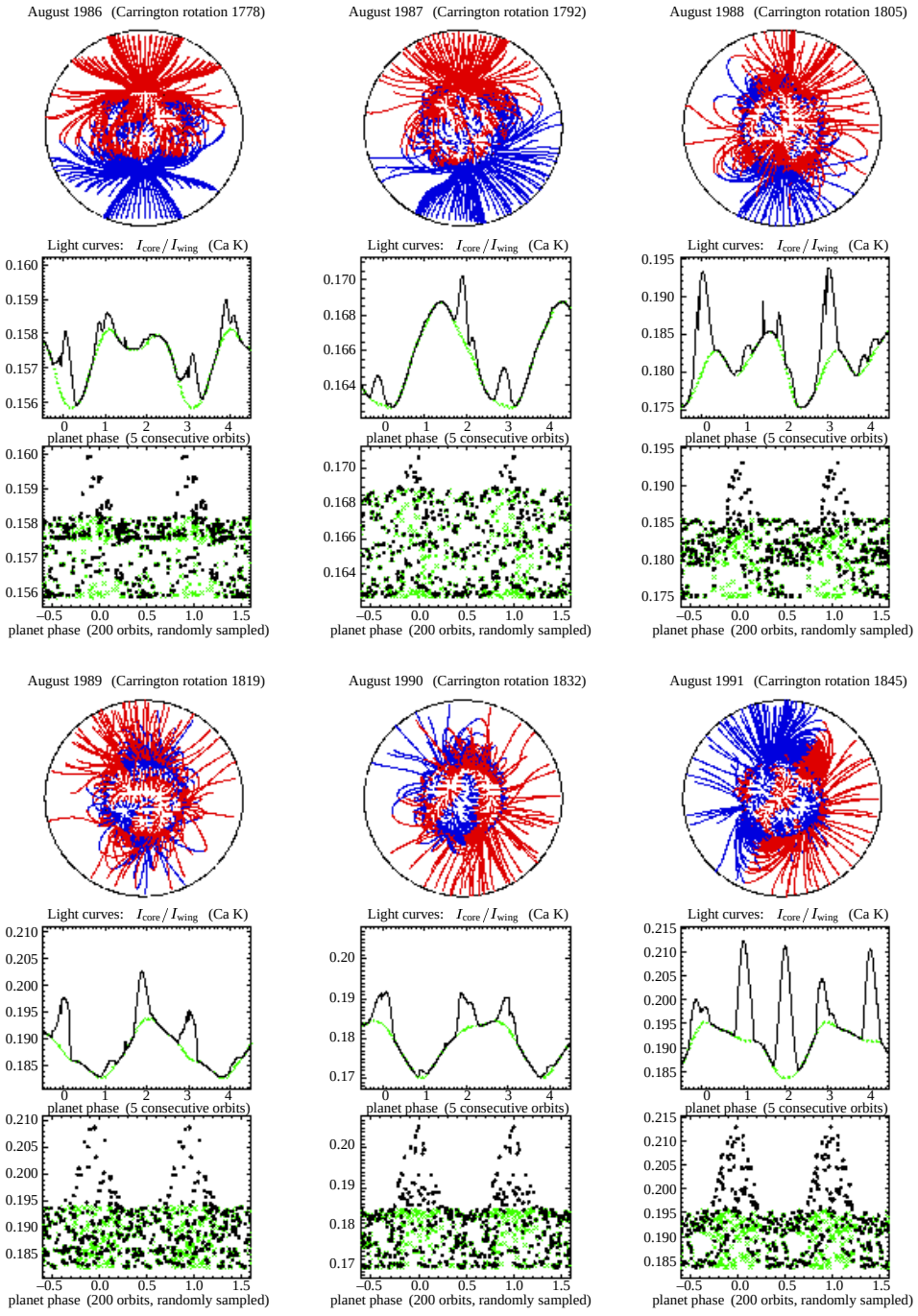

Figure 3. For years 1986–1991, the top panel shows the star's magnetic field out to R_{ss}, with positive [negative] polarity in blue [red]. The middle panel shows a representative light curve over 5 planetary orbits, and the bottom panel shows a coarser random sampling over 200 orbits all phased together. In both, the full star+planet light curve is in black (solid curves, filled circles), and the stellar rotational component only is in green (dotted curves, X's).

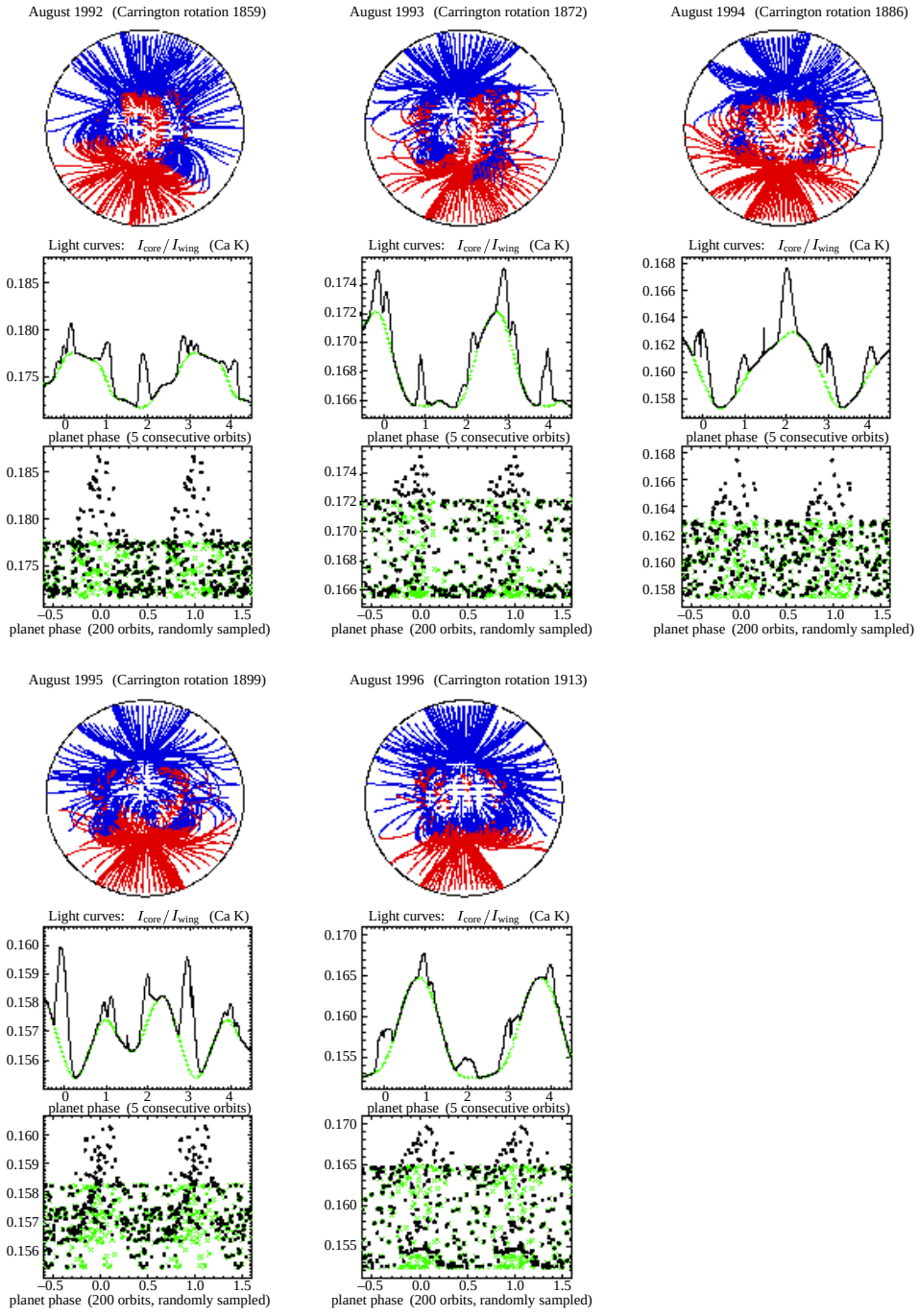

Figure 4. For years 1992–1996, the top panel shows the star's magnetic field out to R_{ss}, with positive [negative] polarity in blue [red]. The middle panel shows a representative light curve over 5 planetary orbits, and the bottom panel shows a coarser random sampling over 200 orbits all phased together. In both, the full star+planet light curve is in black (solid curves, filled circles), and the stellar rotational component only is in green (dotted curves, X's).

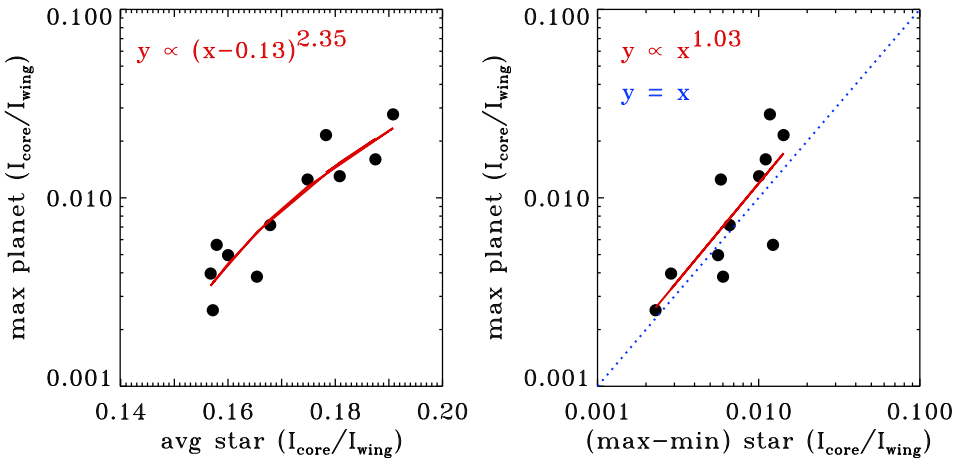

Figure 5. Correlations between statistical properties of the stellar (abscissa) and planetary (ordinate) light curves over the 11 modeled epochs.

Better observational phase coverage (even using multiple observatories to obtain round-the-clock time series) over consecutive orbits and stellar rotations would yield much better tests of the magnetic interaction paradigm. More work needs to be done, of course, to model how the stellar magnetic fields differ from the fiducial solar case modeled here. Additional kinds of observations, such as X-rays that may be phased with the planet's orbit (Saar et al., these proceedings), will help constrain the dynamics and energetics of the interaction.

Acknowledgments. This work was supported by the National Aeronautics and Space Administration (NASA) under grants NNG04GE77G and NNG04-GL54G to the Smithsonian Astrophysical Observatory.

References

Altschuler, M. D., & Newkirk, G., Jr. 1969, Solar Phys., 9, 131
Clarke, J. T., Ajello, J., Ballester, G., et al. 2002, Nature, 415, 997
Cuntz, M., Saar, S. H., & Musielak, Z. E. 2000, ApJ, 533, L151
Ferreira, J. M. & Mendoza-Briceño C. A. 2005, A&A, 433, 1055
Harrington, J., Hansen, B. M., Luszcz, S. H., et al. 2006, Science, 314, 623
Hoeksema, J. T., & Scherrer, P. H. 1986, Solar Phys., 105, 205
Ip, W.-H., Kopp, A., & Hu, J.-H. 2004, ApJ, 602, L53
McIvor, T., Jardine, M., & Holzwarth, V. 2006, MNRAS, 367, L1
Preusse, S., Kopp, A., Büchner, J., & Motschmann, U. 2006, A&A, 460, 317
Rubenstein, E. P., & Schaefer, B. E. 2000, ApJ, 529, 1031
Saar, S. H., Cuntz, M., & Shkolnik, E. 2004, in Stars as Suns: Activity, Evolution and Planets, ed. A. Dupree & A. Benz, Proc. IAU Symp. 219, p. 355
Sánchez-Lavega, A. 2004, ApJ, 609, L87
Schaefer, B. E., King, J. R., & Deliyannis, C. P. 2000, ApJ, 529, 1026
Schatten, K. H., Wilcox, J. M., & Ness, N. F. 1969, Solar Phys., 6, 442
Schrijver, C. J., Coté, J., Zwaan, C., & Saar, S. H. 1989, ApJ, 337, 964
Shibata, K., Masuda, K. S., Shimijo, M., et al. 1995, ApJ, 451, L83
Shkolnik, E., Walker, G. A. H., & Bohlender, D. A. 2003, ApJ, 597, 1092

Shkolnik, E., Walker, G. A. H., Bohlender, D. A., Gu, P.-G., & Kürster, M. 2005, ApJ, 622, 1075
Simon, T., Linsky, J. L., & Schiffer, F. H., III 1980, ApJ, 239, 911
Stevens, I. R. 2005, MNRAS, 356, 1053
Valenti, J. A., & Fischer, D. A. ApJS, 159, 141
Wang, Y.-M., & Sheeley, N. R., Jr. 1990, ApJ, 355, 726
Zarka, P., Treumann, R. A., Ryabov, B. P., & Ryabov, V. B. 2001, Ap&SS, 277, 293